

Optimized Periodic Coulomb Potential in Two Dimension

Markus Holzmann and Bernard Bernu
 Laboratoire de Physique Théorique des Liquides
 UMR 7600 of CNRS
 Université Pierre et Marie Curie
 boîte 121, 4 Place Jussieu
 F-75252 Paris, France

March 22, 2022

Abstract

The $1/r$ Coulomb potential is calculated for a two dimensional system with periodic boundary conditions. Using polynomial splines in real space and a summation in reciprocal space we obtain numerically optimized potentials which allow us efficient calculations of any periodic (long-ranged) potential up to high precision. We discuss the parameter space of the optimized potential for the periodic Coulomb potential. Compared to the analytic Ewald potential, the optimized potentials can reach higher precisions by up to several orders of magnitude. We explicitly give simple expressions for fast calculations of the periodic Coulomb potential where the summation in reciprocal space is reduced to a few terms.

1 Introduction

Most of classical or quantum simulations are using periodic boundary conditions to extrapolate the results to the thermodynamic limit of the bulk. Typically, boundary conditions are implemented by including replicas of the original system; the potentials are then calculated by considering the additional interactions between the particles in the box with all the periodic images of the replicas. Whereas for short-range potentials the nearest image convention can often be applied, long-range potentials require an additional summation over the Fourier components in reciprocal space due to the slow convergence of the contributions of images in real space (see [1] for a recent review of how to compute long range potentials within periodic boundary conditions).

Following Ref. [2], we introduce an optimized periodic potential, represented by two summations, one over Fourier and one over real-space components, which can be obtained numerically for any potential. We extend the analysis of Ref. [2] to treat two-dimensional systems and concentrate particularly on the two-dimensional periodic Coulomb potential.

For an arbitrary potential $v(\mathbf{r})$, the periodic image potential $v_{pp}(\mathbf{r})$ is defined by summing over the interactions between one particle in a box of dimensions L_x, L_y and the replicas of the other particles in periodic space,

$$v_{pp}(\mathbf{r}) = \sum_{\mathbf{l}} v(\mathbf{r} + \mathbf{l}) = \sum_{\mathbf{k}} \tilde{v}_{\mathbf{k}} e^{i\mathbf{k} \cdot \mathbf{r}} \quad (1)$$

Here, \mathbf{l} are the Bravais lattice vectors $(n_x L_x, n_y L_y)$ with n_x, n_y integers, $\tilde{v}_{\mathbf{k}}$ are the Fourier components of the potential summed over all reciprocal lattice vectors $\mathbf{k} = 2\pi(n_x/L_x, n_y/L_y)$ of the periodic system.

For a charge q , the Coulomb potential is given by

$$v(r) = \frac{q}{r} - \int_V d\mathbf{r}' \frac{q}{|\mathbf{r} - \mathbf{r}'|}, \quad (2)$$

with Fourier components

$$\tilde{v}_k = \begin{cases} \frac{1}{V} \frac{2\pi q}{k} & : k \neq 0 \\ 0 & : k = 0 \end{cases} \quad (3)$$

in two dimensions where $V = L_x L_y$ is the volume of the box. A uniform background of opposite charge is subtracted to enforce charge-neutrality. Since both summations in real space and in reciprocal space of the periodic potential converge slowly, the standard method is to split the periodic potentials into two summations,

$$v_{op}(\mathbf{r}) = \sum_{\mathbf{l}} w(\mathbf{r} + \mathbf{l}) + \sum_{|\mathbf{k}| \leq K_c} \tilde{y}_{\mathbf{k}} e^{i\mathbf{k} \cdot \mathbf{r}} \quad (4)$$

with

$$w(r) \equiv 0 \quad \text{for } r > R_c. \quad (5)$$

By definition both summations are converged. In Ref. [2] it has been proposed to use a set of basis functions for $w(r)$ and determine numerically their coefficients together with $\tilde{y}_{\mathbf{k}}$ such that the difference between the optimized periodic potential $v_{op}(\mathbf{r})$ and the periodic image potential $v_{pp}(\mathbf{r})$ is minimized.

An analytical form for the Coulomb potential was provided long time ago by Ewald using a Gaussian charge distribution [3]. It gives

$$w^\alpha(r) = q \frac{\text{erfc}(\alpha r)}{r} \quad (6)$$

$$\tilde{y}_k^\alpha = q \begin{cases} \frac{2\pi}{V} \frac{\text{erfc}(k/2\alpha)}{k} & : k \neq 0 \\ -\frac{2\sqrt{\pi}}{\alpha V} & : k = 0 \end{cases} \quad (7)$$

with $\lim_{r \rightarrow 0} w^\alpha(r) - q/r = -q2\alpha/\sqrt{\pi}$ and α is an open parameter which determines the speed of convergence in both summations. Due to the exponential convergence of both summations, they can be truncated, and R_c and K_c can be determined to ensure any desired precision. Choosing $\alpha = \sqrt{\pi/V}$, both summations roughly converge equally fast, and $(R_c K_c)$ is the only parameter determining the precision of the truncated Ewald potential. In practice, one typically restricts $R_c < L/2$ with $L = \min\{L_x, L_y\}$ in order to apply the nearest image convention in real space; the precision of the potential then relies on $\{\alpha, K_c\}$.

In Ref. [2] it has been shown that a numerical fit of the 3D Coulomb potential reduces considerably the number of terms in k-space with respect to the analytical Ewald summation in order to obtain a comparable precisions. This leads to an important speedup of simulations of charged systems. Further, this method is not limited to the Coulomb potential, but can easily be applied to any functional form. This is important in ground state quantum Monte Carlo calculations, since analytical forms for the potentials have been shown to provide an accurate description of the ground state wavefunction of electronic systems [4, 5]; however, they typically involve more complicated (long ranged) functions where no easy analytical break-up can be done. The optimized potential of Ref. [2] has the big advantage to be applicable to all type of function; here, we extend this method to include two-dimensional systems.

In the following section, we shortly remind the basic steps necessary to derive the equations of the optimized potential which have to be solved numerically, and give the explicit formulas for the 2D case. The precise numerical evaluation of Bessel functions and their integrals are discussed. In section III are presented the results of the optimized potential. Explicit simple formulas are given for the 2D periodic Coulomb potential up to a few percents.

2 Method and formulas for 2D

2.1 General method

The optimized potential, v_{opt} , is determined by minimizing the absolute error with respect to the true periodic potential, v_{PP} ,

$$\chi^2 = \frac{1}{L^2} \int_{L^2} d\mathbf{r} [v_{pp}(\mathbf{r}) - v_{op}(\mathbf{r})]^2. \quad (8)$$

Denoting $\tilde{w}_{\mathbf{k}}$ the Fourier transform of $w(\mathbf{r})$ in the optimized potential, Eq.(4) reads

$$v_{op}(\mathbf{r}) = \sum_{\mathbf{k}} e^{i\mathbf{k}\cdot\mathbf{r}} \tilde{w}_{\mathbf{k}} + \sum_{|\mathbf{k}| \leq K_c} e^{i\mathbf{k}\cdot\mathbf{r}} \tilde{y}_{\mathbf{k}}, \quad (9)$$

and Eq.(8) is split in two sums:

$$\chi^2 = \sum_{|\mathbf{k}| \leq K_c} (\tilde{v}_{\mathbf{k}} - \tilde{y}_{\mathbf{k}} - \tilde{w}_{\mathbf{k}})^2 + \sum_{|\mathbf{k}| > K_c} (\tilde{v}_{\mathbf{k}} - w_{\mathbf{k}})^2. \quad (10)$$

The first term on the rhs of this equation can be exactly set to zero determining $\tilde{y}_{\mathbf{k}}$,

$$\tilde{y}_{\mathbf{k}} = \tilde{v}_{\mathbf{k}} - \tilde{w}_{\mathbf{k}} \quad \text{for } |\mathbf{k}| \leq K_c. \quad (11)$$

Expanding $w(\mathbf{r}) = \sum_i t_i c_i(\mathbf{r})$ using a set of basis functions $c_i(\mathbf{r})$ with Fourier components $\tilde{c}_{i\mathbf{k}}$, Eq.(11) relates the optimal Fourier coefficients $y_{\mathbf{k}}$ to the optimal coefficients t_i in real space

$$\tilde{y}_{\mathbf{k}} = \tilde{v}_{\mathbf{k}} - \sum_i t_i \tilde{c}_{i\mathbf{k}} \quad \text{for } |\mathbf{k}| \leq K_c. \quad (12)$$

The optimal coefficients t_i can be determined by minimizing the second term of the rhs of Eq.(10) leading to the following linear equations

$$\sum_n \sum_{|\mathbf{k}| > K_c} \tilde{c}_{i\mathbf{k}} \tilde{c}_{n\mathbf{k}} t_n = \sum_{|\mathbf{k}| > K_c} \tilde{v}_{\mathbf{k}} \tilde{c}_{i\mathbf{k}} \quad (13)$$

Solving Eq.(12) and Eq.(13) uniquely determines the optimized potential for any given R_c and K_c .

2.2 Polynomial Basis set

Here, we use polynomial splines sitting on a linear grid with m continuous derivatives as basis set (assuming a spherical symmetry of the potential). Following Ref.[2], the splines are defined on intervals (r_i, r_{i+1}) with $N_{spline} + 1$ equally spaced knots starting at the origin and ending at R_c , $r_i = i\Delta$ with interval $\Delta = R_c/N_{spline}$. The basis functions are $c_{i\alpha}(r)$ with $0 \leq \alpha \leq m$ are defined by imposing

$$\left. \frac{d^\beta c_{i\alpha}(r)}{dr^\beta} \right|_{r=r_j} = \delta_{\alpha\beta} \delta_{ij}. \quad (14)$$

The divergence of the potential at the origin is explicitly taken in to account as follow,

$$w(r) = \sum_{i=0}^{N_{spline}} \sum_{\alpha=0}^m t_{i\alpha} \frac{c_{i\alpha}(r)}{r^C} \quad (15)$$

where $C = 1$ for the Coulomb potential and $C = 0$ for regular potential at the origin. Thus, the basis functions $c_{i\alpha}(r)$ are piecewise polynomial of order $2m + 1$

$$c_{i\alpha}(r) = \begin{cases} \Delta^\alpha \sum_{n=0}^{2m+1} S_{\alpha n} \left(\frac{r-r_i}{\Delta} \right)^n & : r_i < r \leq r_{i+1} \\ (-\Delta)^\alpha \sum_{n=0}^{2m+1} S_{\alpha n} \left(\frac{r_i-r}{\Delta} \right)^n & : r_{i-1} < r \leq r_i \end{cases} \quad (16)$$

and zero for $|r - r_i| > \Delta$. The constraints at $r = r_i$ fixe half of the S -elements

$$S_{\alpha n} = \frac{1}{n!} \delta_{\alpha, n}, \quad \text{for } 0 \leq \alpha, n \leq m. \quad (17)$$

The constraints at $r = r_{i\pm 1}$ gives

$$S_{\alpha, n+m+1} = - \sum_{k=0}^{\alpha} (M^{-1})_{kn} \frac{1}{(\alpha - k)!} \quad \text{for } 0 \leq \alpha, n \leq m \quad (18)$$

where M^{-1} is the inverse of the quadratic matrix

$$M_{ak} = \frac{(m+1+a)!}{(m+1+a-k)!} \quad \text{for } 0 \leq a, k \leq m. \quad (19)$$

The required Fourier coefficients $\tilde{c}_{i\alpha k}$ are given by

$$\tilde{c}_{i\alpha k} = \Delta^{\alpha} \sum_{n=0}^{2m+1} S_{\alpha n} (D_{ikn}^{+} + (-1)^{\alpha+n} D_{ikn}^{-}) \quad (20)$$

where

$$D_{ikn}^{\pm} = \pm \frac{1}{V} \int_{r_i}^{r_{i\pm 1}} d\mathbf{r} e^{-i\mathbf{k} \cdot \mathbf{r}} r^{-C} \left(\frac{r - r_i}{\Delta} \right)^n \quad (21)$$

$$= \pm \frac{1}{V \Delta^n} \sum_{j=0}^n \binom{n}{j} (-r_i)^{n-j} \int_{r_i}^{r_{i\pm 1}} d\mathbf{r} r^{j-C} e^{-i\mathbf{k} \cdot \mathbf{r}} \quad (22)$$

$$= \pm \frac{2\pi}{V \Delta^n} \sum_{j=0}^n \binom{n}{j} (-r_i)^{n-j} \int_{r_i}^{r_{i\pm 1}} dr r^{j+1-C} J_0(kr) \quad (23)$$

with $J_0(x)$ is the Bessel function of zero order and $\binom{n}{j}$ denotes the binomial coefficients. The moments of J_0 can be obtained from its first two moments and a recurrence relation:

$$\int dx J_0(x) = x J_0(x) + \frac{\pi}{2} (H_0(x) J_1(x) - H_1(x) J_0(x)) \quad (24)$$

$$\int dx x J_0(x) = x J_1(x) \quad (25)$$

$$\int dx x^n J_0(x) = x^n J_1(x) + (n-1) x^{n-1} J_0(x) - (n-1)^2 \int dx x^{n-2} J_0(x). \quad (26)$$

Here, J_1 is the Bessel function of first order and H_1 (H_2) is Struve's function of first (second) order. However, contrary to the 3D case, we have not found any "machine precision" routine to compute the Struve's function or the integral of J_0 due to the oscillatory behavior of the integrand. In Appendix A, we briefly describe how to evaluate "precisely" the integral of J_0 .

3 Results for the 2D periodic Coulomb potential

In this section, we present the results of the optimized potential for the Coulomb $1/r$ potential in two dimensions, Eq.(2) and Eq.(3) in a square box of length $L = L_x = L_y$. Hermite splines of fifth order represent the real space part of the optimized potential insuring two continuous derivatives ($m = 2$ in Eq.16). The $1/r$ divergence at the origin is accounted for by setting $C = 1$ with the constraint $t_{i=0, \alpha=0} = q$; symmetry further imposes the absence of any linear term linear: $t_{i=0, \alpha=2} = 0$. Both constraints can be easily included, by solving the linear equations

$$\sum_{(j, \beta) \neq \{(0,0), (0,2)\}} A_{i\alpha, j\beta} t_{j\beta} = b_{i\alpha}, \quad 0 \leq \alpha \leq m_{nderv}, \quad 0 \leq i \leq N_{spline} \quad (27)$$

for $(i, \alpha) \neq \{(0, 0), (0, 2)\}$ with

$$A_{i\alpha, j\beta} = \sum_{k=K_c}^{K_m} \tilde{c}_{i\alpha k} \tilde{c}_{j\beta k} \quad b_{i\alpha} = \sum_{k=K_c}^{K_m} (\tilde{v}_k - \tilde{c}_{00k} t_{00}) \tilde{c}_{i\alpha k} \quad (28)$$

instead of Eq.(13). Appendix B describes how to impose the Madelung constant of the lattice through the constant term t_{01} .

The number of spline intervals, N_{spline} , and the cut-off K_c in the reciprocal space are the open parameters of the model. In Eq.(28), K_m has to be large enough to insure that each sum is converged. Since it is an important parameter which determines the conditioning of the linear equation we first discuss its influence on the stability of the solution.

The results of the optimized potential are compared with the “exact” periodic Coulomb potential obtained from the Ewald formula including a summation over many images in real space. Thus machine precision is easily reached for this reference potential. Values of the potential are given in units of q/L , they are independent of the size of the box.

3.1 Extrapolation of K_m

Results are very sensitive to K_m which determines the convergence of the matrix elements of A and b , Eq.(28). From Eq.(20) and Eq.(23), one finds the dominant behavior in the limit of $k \rightarrow \infty$: $t_{00}\tilde{c}_{00k} - \tilde{v}_k \sim \mathcal{O}(k^{-7/2})$ and $\tilde{c}_{i\alpha k} \sim \mathcal{O}(k^{-7/2})$ for $(i, \alpha) \neq (0, 0)$. Thus the matrix elements in A and b , Eq.(28), are of order k^{-7} . In the large k limit, the truncation therefore introduces an error of order K_m^{-5} .

Considering the asymptotic expansions of $c_{i\alpha k}$ for large k , one might be able to extend the summation analytically to infinity using the leading order terms. However, in 2D, the difference between the discrete summation over reciprocal lattice vectors and the continuous integration is comparable to the correction of the continuous integral. Therefore, we find no improvement by adding those corrections. Thus, contrary to the 3D case, no analytical continuations are used here.

Next, we consider the stability of the solution with respect to variations of K_m . Since the short wavelength cut-off destroys the information on small distance behavior of the potential, we expect that there is a maximum number of splines N_{spline}^{max} , after which the solution of the linear equation will become unstable. Roughly, the resolution in real space is limited by $\Delta K_m / (2m + 2) > \sim 2\pi$, and we get a maximum number of spline knots $N_{spline}^{max} + 1$ with

$$N_{spline}^{max} \leq \frac{K_m R_c}{4\pi(m+1)} \quad (29)$$

Using less terms in the summation in reciprocal space, the matrix $A_{i\alpha j\beta}$ in Eq.(28) becomes ill conditioned. The conditioning of the linear system can be estimated by comparing the norm of the obtained solution t_i , $\|t\|_\infty = \max\{|t_i|, i\}$ with $\|s\|_\infty = \max\{|\sum_j A_{ij} t_j - b_i|, i\}$. If $\|s\|_\infty / \|t\|_\infty$ is of order one, the system is dominated by numerical round-off errors. This indicates that either the value of K_m is too small or the number of splines is too large so that no improvement can be reached by increasing N_{spline} further.

3.2 Accuracy of the optimized potential

We now study the accuracy of the optimized potential in the $N_{spline} - K_c^2$ -plane for fixed $R_c/L = 0.5$ (nearest image convention). The $\sqrt{\chi^2}$ in units of q/L corresponds to the average error and is shown in Fig. 1. We see that there is an optimum line in the range of parameters considered. We also note that there is a difficulty to decrease the precision below 10^{-10} , mainly because the linear system, Eq.(28) becomes more and more ill-conditioned as N_{spline} and K_c^2 increase.

Figure 2 shows the difference to the true periodic potential for $N_{spline} = 30$ varying K_c^2 and compares it with the values of the best nearest image potential using the analytic Ewald expressions, Eq.(7) with $\alpha = K_c/L$. For the range of interest in order to speed up simulations,

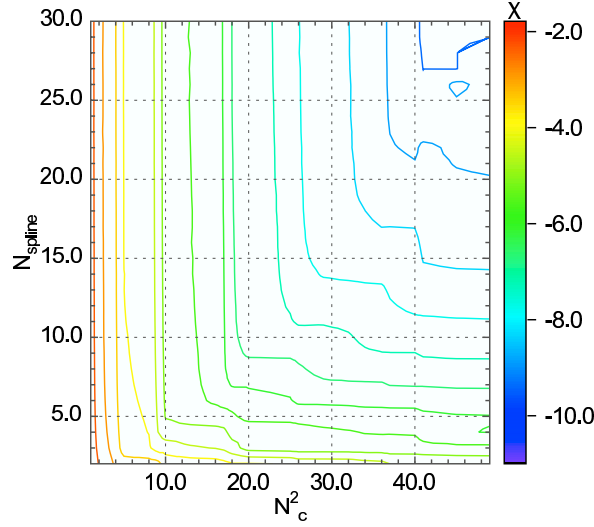


Figure 1: Contour plot of the mean error of the optimized potential versus the number of shells N_c^2 ($N_c = K_c L / 2\pi$) and the number of splines N_{spline} (see definition of Eq.(4)). The maximum distance in r-space is chosen to satisfy the nearest image convention in simulations, $R_c/L = 0.5$.

the optimized potential is always better by at least one order of magnitude. However, if very high precision is needed, better than 10^{-10} , the Ewald method is preferable to the present optimized procedure, even if it is much more cpu-time consuming, since it has no stability problems.

The number of splines increases the precision of the potential inside the circle of radius R_c . Around the corner of the box, only the number of k -shells can improve the optimized potential. At fixed number of shells, one reaches rapidly an optimum number of splines after which increasing the number of splines has no more effect. This is seen in Fig.2 by the straight vertical lines. At fixed number of splines, increasing the number of k -shells first improves strongly the optimized potential, but later the improvement almost saturates. Thus the optimum choice is to take the parameters roughly along the diagonal in Fig.2.

Note that an intermediate precision of 10^{-3} to 10^{-6} is reached with very small values of the optimized potential parameters. Therefore simple analytical expressions allow us fast evaluations of the periodic Coulomb potential with intermediate precisions.

3.3 Simple expressions for intermediate precision

If we include only the first five wavevectors with $|\mathbf{k}| \leq K_c = 2\pi/L$ and use $N_{spline} = 2$, the minimum to obtain a smooth curve going to zero at half of the box size, a mean precision of 1% is obtained. and a maximum error of around 2% (see Table 3.3). Increasing the number of splines improves slightly the precision. However, extending for $N_{spline} = 2$ the reciprocal summation using $K_c = 4\pi/L$, the precision decreases to 0.1%, with a maximum error of 0.4% (see Table 3.3). The short-range part of the optimized Coulomb potential writes

$$w(r) = \frac{q}{r} \begin{cases} \sum_{i=0}^6 a_i^< \left(\frac{4r}{L}\right)^i & : 0 \leq r < L/4 \\ \sum_{i=0}^6 a_i^> \left(\frac{4r}{L} - 1\right)^i & : L/4 \leq r < L/2 \end{cases} \quad (30)$$

whereas the long-range part is given by

$$y(r) = \frac{q}{L} \{ \tilde{y}_0 + 2\tilde{y}_1 [\cos(\hat{x}) + \cos(\hat{y})] + 4\tilde{y}_2 \cos(\hat{x}) \cos(\hat{y}) + 2\tilde{y}_4 [\cos(2\hat{x}) + \cos(2\hat{y})] \} \quad (31)$$

where $\hat{x} = 2\pi x/L$, $\hat{y} = 2\pi y/L$. See Fig.3 for a comparison of these simple expression with the “exact” periodic potential.

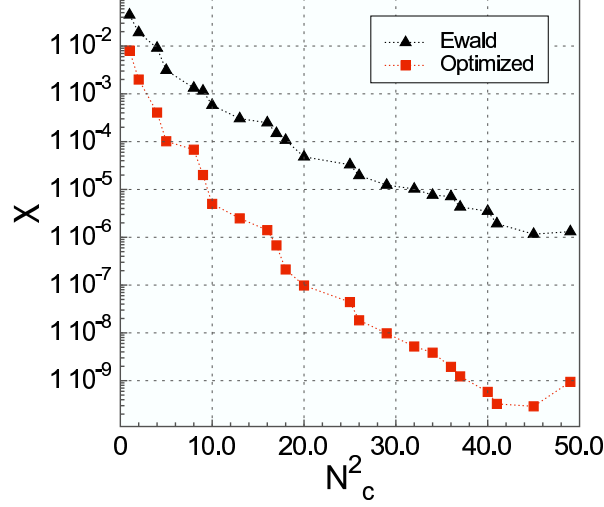


Figure 2: Comparison of the precision between the standard Ewald method (with $\alpha = K_c/L$) (triangle) and the the optimized potential versus $N_c = K_c L/2\pi$ (square). The average error χ is given in units of q/L . The maximum distance in r-space is chosen to satisfy the nearest image convention, $R_c/L = 0.5$.

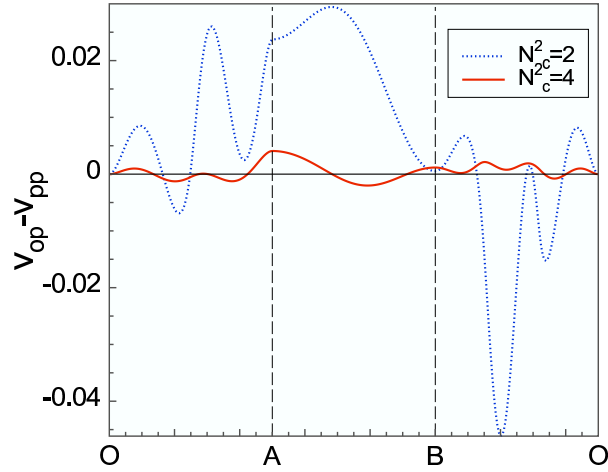


Figure 3: Difference between the simple expression of the optimized potential, v_{op} , with the exact Coulomb potential, v_{pp} ; dooted lined stands for v_{op} using $K_c = 4\pi/L$, full line for $K_c = 8\pi/L$. O stands for the origin, A for the middle of the square side and B for the corner of the square.

i	0	1	2	3	4	5
$a_i^<$	1	-0.819506	0	0.169304	-0.146967	0.0777952
$a_i^>$	0.280626	-0.510485	0.404063	-0.955541	1.3377	-0.556365
n^2	0	1				
\tilde{y}_{n^2}	-1.11863	0.124098				

Table 1: Optimized Potential parameters, Eq.(30 and Eq.(31). Top : short range real space parameters for $N_{spline} = 2$. Bottom : reciprocal space parameters where $n = kL/2\pi$. The mean precision is about 2%.

i	0	1	2	3	4	5
$a_i^<$	1	-1.09583	0	0.30778	-0.0359887	-0.0266302
$a_i^>$	0.149336	-0.449592	0.441105	-0.119121	-0.0333851	0.0116568
n^2	0	1	2	4		
\tilde{y}_{n^2}	-0.870938	0.262177	0.0715766	0.00474028		

Table 2: Same as Table 3.3. The mean precision of this model is about 0.1%.

Both explicit expressions are roughly one order of magnitude better than the corresponding Ewald potentials. Even if not extremely precise, the expressions should extrapolate much better to the thermodynamic limit than any truncated potential using only nearest image convention in real space. Further the real space part of the optimized potential vanishes at $R_c = L/2$ by construction without introducing any discontinuity in the potential and the derivatives at this point.

4 Conclusion

We have shown that for the two dimensional Coulomb potential, the numerically optimized potential can obtain a much higher precision compared to the analytical Ewald potential summing over the same number of terms in reciprocal space. Therefore, the computational effort for many-body simulations involving long range potentials can be significantly reduced using an optimized potential.

For a pair potential the computational cost to evaluate the real space contribution to the total potential is $\sim NN_c/2$ where N is the total number of particle, $N_c = \pi R_c^2 \rho$ is the “number of close neighbors” and $\rho = N/V$ the mean particle density. Since the number of k -vectors increases as the volume in reciprocal space, the cost of the Fourier summation is roughly $\sim N\pi K_c^2 V/4\pi^2$, and there is an optimum value for each system size, which scales as $R_c \sim K_c^{-1} \sim N^{1/4} \sim L^{1/2}$ in the limit of a large particle number, so that the computational cost in reciprocal space $\sim N^{3/2}$ roughly equals that in real space. We further note, that in the limit of a large system, the total cost for evaluating the Coulomb potential using real and reciprocal space summations is always favorable compared to any truncated potential with minimum image convention, which scales as $\sim N^2$.

Apart from a potential speed-up of simulations involving charged particles, the big advantage of the optimized potential is its flexibility to split-up any (long-ranged) function into a real-space and a reciprocal space contribution.

Appendix A

In this Appendix, we describe how to evaluate precisely the integral of the Bessel function $J_0(x)$. Beginning with the evaluation of the Bessel function J_0 , three domains are defined. Around the

origin, $0 \leq x \leq x_1$ the Bessel function is accurately evaluated from the absolutely convergent series representation [6]

$$J_0(x) = \sum_{k=0}^{\infty} \left(-\frac{x}{2k!}\right)^{2k}, \quad 0 \leq x \leq x_1 \quad (32)$$

With standard double precision, a precision of 10^{-14} is obtained up to $x_1 = 10$ by summing all terms whose absolute value is larger than 10^{-18} . For large arguments, $x_2 \leq x < \infty$, the asymptotic expansion is used: [6]

$$J_0(x) = \sqrt{\frac{2}{\pi x}} [P(x) \cos(x - \pi/4) + Q(x) \sin(x - \pi/4)], \quad x_2 \leq x < \infty \quad (33)$$

with

$$P(x) = 1 + \sum_{k=1} \frac{(-1)^k}{(8x)^{2k}} \prod_{m=0}^{2k-1} \frac{(2m+1)^2}{(m+1)}, \quad Q(x) = \sum_{k=0} \frac{(-1)^k}{(8x)^{2k+1}} \prod_{m=0}^{2k} \frac{(2m+1)^2}{(m+1)} \quad (34)$$

As usual, the summation is stopped when the absolute value of the running term of the series starts to increase. With the asked precision of 10^{-14} , one finds $x_2 = 16$. In the intermediate region $x_1 < x < x_2$, the Chebyshev-pade approximant are calculated using Maple. This strategy can be extended to any desired precision by cutting this interval in pieces.

The series expressions for $J_0(x)$ are then analytically integrated to calculate $\int dx J_0(x)$. Unfortunately, the asymptotic expression is less converging, giving $x_2 = 30$ for a precision of 10^{-14} . The Chebyshev-pade approximant in the interval $[10, 30]$ is calculated at order 36, thanks to Maple: *with(orthopoly): with(numapprox): Digits:=20; IJ:=int(BesselJ(0,x),x); IJCh:=eval(chebpade(IJ, x=10..30,36)): convert(subs(x=10*(X+2),IJCh),horner);* where $X = (x - 20)/10$. The *gsl* routine have been used for J_0 and J_1 [7].

Appendix B

It is also possible to fix the constant term at the origin in the optimized Coulomb potential, t_{01} in Eq.(15), by imposing the Madelung constant of the underlying lattice, $v_{Mad} = \lim_{r \rightarrow 0} (v_{PP}(r) - q/r)$. Using the Ewald expressions, Eq.(7), the Madelung constant writes

$$v_{Mad} = \sum_{\mathbf{l} \neq (0,0)} w^\alpha(\mathbf{l}) + \sum_{\mathbf{k}} \tilde{y}_{\mathbf{k}}^\alpha - 2\sqrt{\frac{\alpha}{\pi}} \quad (35)$$

which can be calculated with high precision choosing $\alpha = \sqrt{\pi}/L$; for the square lattice $v_{Mad} = -3.90026492000195q/L$. For the optimized potential, imposing the $1/r$ divergency with $C = 1$, the Madelung verifies $v_{Mad} = t_{01} + \sum_{k \leq K_c} \tilde{y}_k$. Since \tilde{y}_k is coupled to all $t_{i\alpha}$ by Eq.(12), this constraint leads to modifications of Eq.(28),

$$\sum_{(j,\beta) \neq \{(0,0), (0,1), (0,2)\}} A_{i\alpha,j\beta} t_{j\beta} = b_{i\alpha}, \quad 0 \leq \alpha \leq m, \quad 0 \leq i \leq N_{spline} \quad (36)$$

for $(i, \alpha) \neq \{(0,0), (0,1), (0,2)\}$ with

$$A_{i\alpha,j\beta} = \sum_{k=K_c}^{K_m} \tilde{c}_{i\alpha k} \tilde{c}_{i\beta k} \quad (37)$$

$$b_{i\alpha} = \sum_{k=K_c}^{K_m} \left(\tilde{v}_k - \tilde{c}_{00k} t_{00} - \tilde{c}_{10k} \frac{v_{Mad}}{1 - \sum_{q \leq K_c} \tilde{c}_{10q}} - \sum_{j\beta \neq (0,1)} t_{j\beta} (\tilde{c}_{j\beta q} - \tilde{c}_{j\beta q}) \right) \tilde{c}_{i\alpha k} \quad (38)$$

$$\tilde{\tilde{X}}_k = \tilde{X}_k + \tilde{c}_{10k} \frac{\sum_{q \leq K_c} \tilde{X}_q}{1 - \sum_{q \leq K_c} \tilde{c}_{10q}} \quad (39)$$

instead of Eq.(13). Here X denotes either $c_{i\alpha}$ or v . Including the Madelung term as a constraint improves slightly the solution.

ACKNOWLEDGMENTS: We acknowledge discussions with D. Ceperley. M.H. is grateful to S. Chiesa for providing the 3D-version of the optimized potential used for comparisons.

References

- [1] C. Holm, NICSeries, Vol. 23, ISBN3-00-012641-4, pp. 195, (2004).
- [2] V. Natoli and D. Ceperley, J. Comput. Phys. **117**,171 (1995).
- [3] P.P. Ewald, Ann. Phys. **64**, 253 (1921). Mike P. Allen and Dominik J. Tildesley. “Computer Simulation of Liquids”. Oxford Science Publications. Clarendon Press, Oxford, 1 edition, 1987.
- [4] D. Ceperley, Phys. Rev. **B 18**, 3126 (1978).
- [5] M. Holzmann, D. M. Ceperley, C. Pierleoni, and K. Esler, Phys. Rev E **68**, 046707 (2003).
- [6] *Handbook of Mathematical Functions*, edited by M. Abramowitz and I. A. Stegun, Dover Publications, New York (1970).
- [7] <http://sources.redhat.com/gsl/>